Journal of Sound and Vibration 325 (2009) 705–721

Contents lists available at ScienceDirect

Journal of Sound and Vibration

journal homepage: www.elsevier.com/locate/jsvi

Embedded absorbers for helicopter rotor lag damping

Lynn Byers, Farhan Gandhi *

Vertical Lift Research Center of Excellence, Department of Aerospace Engineering, The Pennsylvania State University, University Park, PA 16802, USA

ARTICLE INFO

Article history:
Received 6 January 2007
Received in revised form
23 March 2009
Accepted 24 March 2009
Handling Editor: C.L. Morfey
Available online 25 April 2009

ABSTRACT

Radial and chordwise damped vibration absorbers embedded in the rotor blade are compared for rotor lag damping augmentation. Results show that the radial absorber is more effective in transferring damping to the rotor blade lag mode. The chordwise absorber needs to be at a more outboard location and have a larger mass to introduce levels of lag damping comparable to that introduced by the radial absorber. The 1/rev amplitude of a chordwise absorber at the blade tip, per degree of blade lead-lag motion in forward flight, is of the order of 35% of the blade chord, and such a stroke might be difficult to accommodate. The 1/rev amplitude of a radial absorber at 70% span (having significantly lower mass than the chordwise absorber and producing comparable lag damping) is of the order of 4% of the rotor blade span. The static displacement of the radial absorber under centrifugal load needs to be limited using a frequency-dependent (high static stiffness, low dynamic stiffness) or nonlinear spring. The chordwise absorber can also undergo a large static displacement under the chordwise component of the centrifugal load if there is an offset from the feather axis, and this would again have to be limited using a strategy such as a frequency-dependent spring. Significant advantages of the radial absorber are—higher lag damping, lower absorber mass, space for absorber mass travel, and no chordwise travel of blade center of gravity reducing susceptibility to aeroelastic instability and dynamic pitch-link loads.

1. Introduction

Helicopters with soft-inplane rotors are known to be susceptible to aeromechanical instabilities such as ground- and air-resonance, which arise due to the coupling of the poorly damped rotor cyclic lag modes with the fuselage modes [1–3]. The conventional approach to alleviating these instabilities has been to ensure an adequate amount of damping in the lag mode through the provision of auxiliary lag dampers at the rotor blade root. Early helicopters were equipped with hydraulic root-end lag dampers, but recent years have also seen the widespread use of elastomeric lag dampers on modern rotors. These have been installed on several helicopters including the Boeing AH-64 Apache and the Bell 412. All auxiliary root-end lag dampers (hydraulic or elastomeric) increase hub complexity and aerodynamic drag. While modern elastomeric dampers are less maintenance intensive (free of seals, leaks, and moving parts), they are themselves expensive, susceptible to fatigue, and display complex behavior including nonlinear amplitude dependence, frequency dependence, sensitivity to temperature with loss of damping at extremes in temperature, and blade limit cycle oscillations [4–9]. Although not currently found on any operational helicopters, a good deal of research has recently focused on electrorheological (ER) and magnetorheological (MR) helicopter lag dampers [10–15]. One of the major advantages of ER and MR dampers is the ability

* Corresponding author.
E-mail address: fgandhi@psu.edu (F. Gandhi).

0022-460X/$ - see front matter © 2009 Elsevier Ltd. All rights reserved.
doi:10.1016/j.jsv.2009.03.031

Nomenclature

$\bar{a}$	absorber offset from hub (nondimensionalized by blade length, *R-e*)
$\bar{a}_c$	initial (undeformed) position of chordwise absorber relative to the blade feathering axis (nondimensionalized by blade length, *R-e*)
e	blade lag hinge offset
k_a	absorber spring stiffness
m	blade mass per unit length
m_a	absorber mass
M	total blade mass
$\bar{M}_\zeta$	aerodynamic lag moment
$\bar{x}_c$	chordwise motion of the absorber mass (nondimensionalized by the blade length, *R-e*)
$\bar{x}_r$	radial motion of the absorber mass (nondimensionalized by the blade length, *R-e*)
α_f	frequency ratio (ratio of the absorber rotating natural frequency to the rotating lag frequency)
α_m	mass ratio (ratio of absorber mass, m_a, to blade mass, M)
ν_ζ	blade nondimensional rotating lag frequency
ζ	blade lag dof
ζ_a	absorber damping ratio
ω_ζ	blade rotating lag frequency
$\omega_{\zeta 0}$	blade nonrotating lag frequency
Ω	rotor speed
$\dot{()} = \Omega ()^*$, $\ddot{()} = \Omega^2 ()^{**}$, and $()^* = \mathrm{d}()/\mathrm{d}\psi$	terms used to nondimensionalize equations of motion

to provide increased damping when required, while decreasing it at other times to reduce damper and blade loads. Passive aeromechanical stability augmentation efforts not based on root-end auxiliary dampers have largely focused on designing aeroelastic couplings (pitch-flap, pitch-lag, and flap-lag couplings) into the rotor [16–20]. Although the aeromechanical stability characteristics can be improved considerably, it appears to be difficult to realize adequate stability margins over the entire flight envelope. Recently, embedded damped vibration absorbers within the rotor blade have been investigated for provision of rotor lag damping, and this is discussed in the following section.

2. Embedded vibration absorbers for rotor lag damping

An alternative to root-end auxiliary lag dampers suggested by researchers at Penn State [21–24] was to introduce lag mode damping through an *embedded chordwise damped vibration absorber* in the outboard region of the blade (see Figs. 1 and 2). For the correct choice of system design parameters, it was shown that a significant amount of lag damping could be introduced, and aeromechanical stability could be improved. However, the chordwise absorber has stringent restrictions on stroke-length due to space limitations, and there are concerns that the motion of the absorber mass in the chordwise direction, which results in the movement of the blade center of gravity, can have a detrimental influence on blade aeroelastic stability (pitch-flap flutter) and potentially increase the dynamic pitch link loads. Additionally, the magnitude of the absorber mass required for satisfactory damping augmentation is quite large (on the order of 10% of the blade mass).

More recently, a *radial vibration absorber* has been proposed for its ability to augment rotor blade lag mode damping [25–27]. As depicted in the schematic in Fig. 3, the absorber mass (restrained by a damped spring) oscillates along the spanwise direction (potentially along a frictionless track within the blade leading-edge spar). In the process, it exerts a tangential Coriolis force on the rotating blade in the lead-lag direction. The lead-lag motion of the rotating blade (and the absorber mass), in turn, exerts a radial Coriolis force on the absorber mass (see Fig. 4). Thus, there exists a Coriolis coupling between the lead-lag motion of the blade and the radial motion of the absorber mass. For the damped absorber under

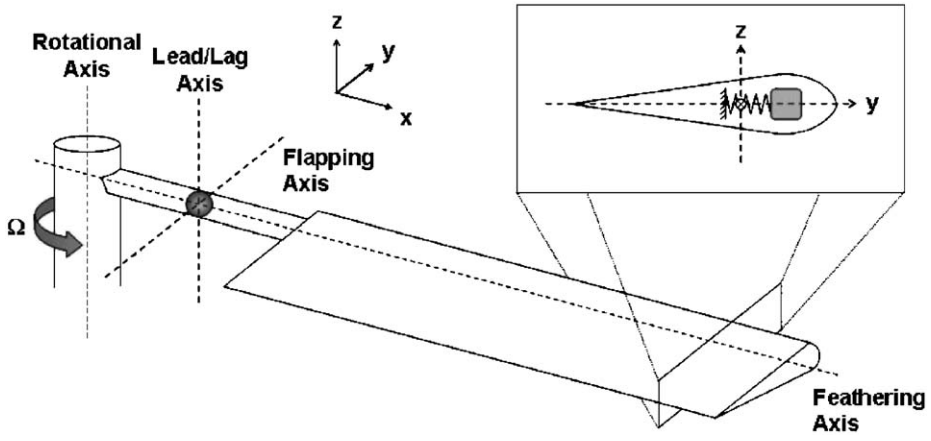

Fig. 1. Embedded chordwise damped vibration absorber [22].

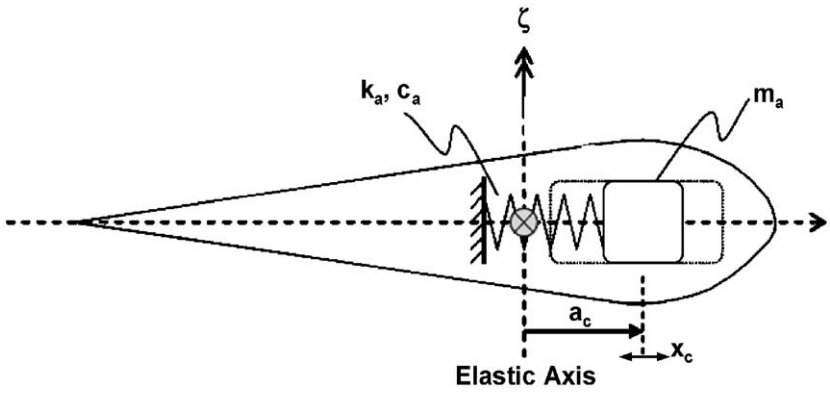

Fig. 2. Embedded chordwise vibration absorber schematic (redrawn from [24]).

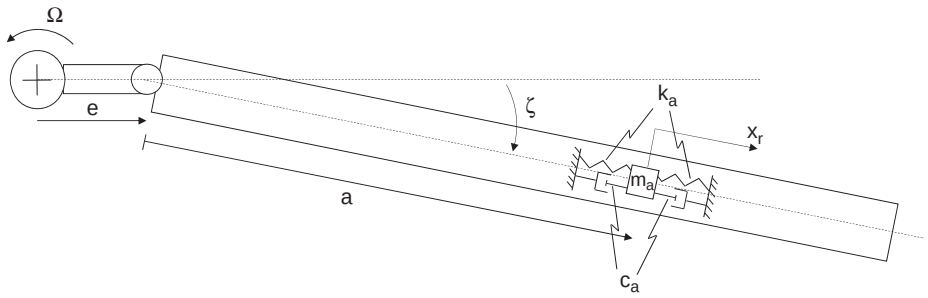

Fig. 3. Embedded radial vibration absorber schematic.

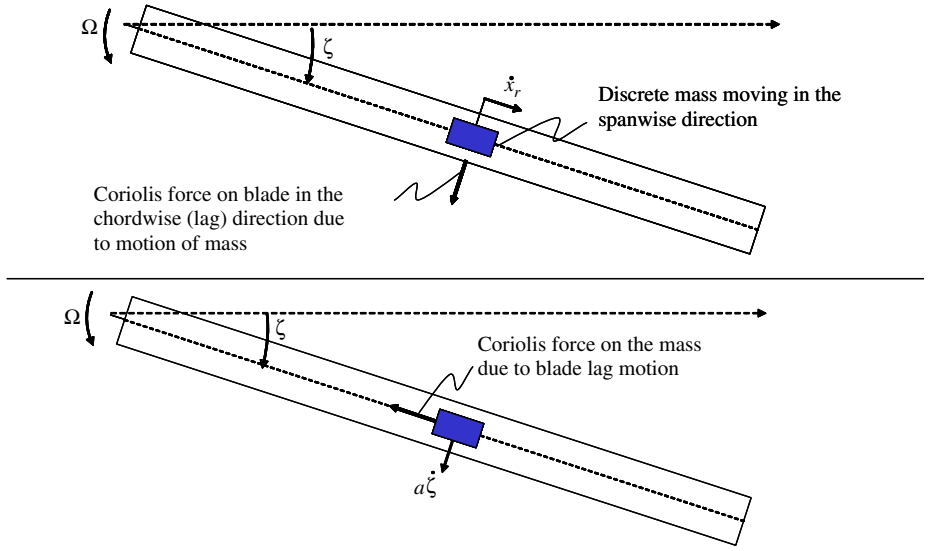

Fig. 4. Coriolis force on blade and absorber mass.

consideration, a significant amount of damping can be transferred into the rotor lag mode through this strong Coriolis coupling.

Relative to the chordwise vibration absorber there are no stringent stroke restrictions for the radial vibration absorber, and it was shown that a modest absorber mass (of the order of 1–5% of the blade mass) could introduce a substantial amount of damping in the rotor lag mode and could easily alleviate aeromechanical instabilities of a hingeless rotor helicopter [25,27]. Since there is no chordwise movement of the center of gravity, susceptibility to pitch-flap flutter instabilities is also reduced.

Previous studies on the chordwise absorber [21,22] and radial absorber [25–27] have been carried out on different rotors, using different absorber parameters. By considering a common rotor and equivalent absorber parameters, the present study seeks to compare the performance of the chordwise and radial absorbers. In particular, the levels of lag damping achieved using both types of absorbers, and the corresponding periodic response amplitudes of the absorber masses for a periodic lead-lag motion of the blade (as would be expected in forward flight conditions) are compared.

3. Analysis of radial and chordwise vibration absorbers

The lag damping results presented in [21,22] for the chordwise absorber cannot be directly compared with the results from [25,27] for the radial absorber since the two absorber concepts are analyzed using different absorber parameters and different rotor systems. In this paper, both chordwise and radial damped vibration absorber concepts are analyzed using similar nondimensional formulations of the differential equations of motion, for similar ranges of absorber parameters. The results compare the amount of lag damping achieved by the radial absorber vs chordwise absorber on the *same rotor*. The study also compares the periodic absorber response amplitudes for periodic lead-lag motion of the blade.

The governing linearized, nondimensional differential equations of motion for the radial absorber are as follows (see Appendix A for a derivation of these equations of motion):

$$\begin{bmatrix} 1+3\alpha_m\bar{a}^2 & 0 \\ 0 & 1 \end{bmatrix} \begin{Bmatrix} \overset{**}{\zeta} \\ \overset{**}{\bar{x}_r} \end{Bmatrix} + \begin{bmatrix} 0 & -6\alpha_m\bar{a} \\ 2\bar{a} & 2\zeta_a\alpha_f v_\zeta \end{bmatrix} \begin{Bmatrix} \overset{*}{\zeta} \\ \overset{*}{\bar{x}_r} \end{Bmatrix} + \begin{bmatrix} v_\zeta^2 & 0 \\ 0 & \alpha_f^2 v_\zeta^2 \end{bmatrix} \begin{Bmatrix} \zeta \\ \bar{x}_r \end{Bmatrix} = \begin{Bmatrix} \bar{M}_\zeta \\ \bar{a} \end{Bmatrix}. \tag{1}$$

In the above equations ζ and $\bar{\boldsymbol{x}}_{\boldsymbol{r}}$ are the rotor lag and the absorber radial dof (as shown in Figs. 3 and 4), α_m is the mass ratio (ratio of absorber mass to blade mass), α_f is the frequency ratio (ratio of the absorber rotating natural frequency to the blade rotating lag frequency), $\bar{a}$ is the absorber offset from lag hinge (nondimensionalized by the blade length, R-e), and ζ_a is the absorber damping ratio. The rotor blade parameter in the above equations is v_ζ (the nondimensional rotating lag frequency), and $\bar{M}_\zeta$ represents the aerodynamic lag moment.

The linearized, nondimensional equations of motion for the chordwise absorber are similarly derived using [22], following a derivation process similar to the radial absorber described in Appendix A, resulting in the following equations:

$$\begin{bmatrix} 1+3\alpha_m\bar{a}^2 & -3\alpha_m\bar{a} \\ -\bar{a} & 1 \end{bmatrix} \begin{Bmatrix} \overset{**}{\zeta} \\ \overset{**}{\bar{x}_c} \end{Bmatrix} + \begin{bmatrix} 0 & 0 \\ 0 & 2\zeta_a\alpha_f v_\zeta \end{bmatrix} \begin{Bmatrix} \overset{*}{\zeta} \\ \overset{*}{\bar{x}_c} \end{Bmatrix} + \begin{bmatrix} v_\zeta^2 & 0 \\ 0 & \alpha_f^2 v_\zeta^2 \end{bmatrix} \begin{Bmatrix} \zeta \\ \bar{x}_c \end{Bmatrix} = \begin{Bmatrix} \bar{M}_\zeta \\ \bar{a}_c \end{Bmatrix}. \tag{2}$$

In Eq. (2), $\bar{x}_c$ is the chordwise motion of the absorber mass (Fig. 2), nondimensionalized by the rotor radius. The remaining absorber and rotor parameters in Eq. (2) are identical to those in Eq. (1), described above.

For both absorber concepts, the absorber rotating natural frequency is determined by the following equation:

$$\omega_a = \sqrt{\frac{k_a}{m_a} - \Omega^2}, \tag{3}$$

where k_a and m_a represent the absorber stiffness and mass. Therefore, the frequency ratio, α_f, for both concepts, is as follows:

$$\alpha_f = \frac{\omega_a}{\omega_\zeta} = \sqrt{\frac{\dfrac{k_a}{m_a} - \Omega^2}{\omega_{\zeta 0}^2 + e\dfrac{S_\zeta}{I_\zeta}\Omega^2}}. \tag{4}$$

As seen in Eqs. (3) and (4), both the absorber rotating natural frequency and the lag natural frequency are functions of rotor speed, Ω. Consequently, for fixed values for the absorber stiffness, k_a, and mass, m_a, the absorber frequency can only be "tuned" to the lag frequency ($\alpha_f = 1$) at a single value of Ω.

For both systems of equations, by setting the forcing terms on the right-hand side to zero and conducting an eigenanalysis, the modal damping of the coupled rotor lag and absorber modes can be calculated. Further, by introducing a harmonic excitation force for the lag equation of motion, frequency response functions (FRFs) for the absorber displacement, $\bar{x}_r$ and $\bar{x}_c$, and blade lag displacement, ζ, can be obtained. The frequency response functions can then be used to calculate the amplitude of the absorber displacement (or the stroke-length of the absorber mass) per degree amplitude of blade lag motion, when the blade is undergoing periodic lead-lag motion in forward flight conditions.

4. Results and discussion

The absorber parameters used for the simulation results presented in this section are given in Table 1. The rotor nondimensional lag frequency, v_ζ, is taken to be 0.7/rev, which is typical of a soft-inplane hingeless rotor.

Figs. 5–7 show the modal damping results, vs frequency ratio, for a moderately damped absorber ($\zeta_a = 0.3$) at inboard ($\bar{a} = 0.3$, Fig. 5), mid-span ($\bar{a} = 0.5$, Fig. 6), and outboard ($\bar{a} = 0.7$, Fig. 7) spanwise locations. For the radial absorber it is

Table 1
Absorber parameters used in simulations.

Absorber parameter	Values considered
$\bar{a}$	0.3, 0.5, 0.7
ζ_a	0.3, 0.5, 0.7
α_f	0.5–1.5
α_m	0.01, 0.02, 0.03, 0.04, 0.05

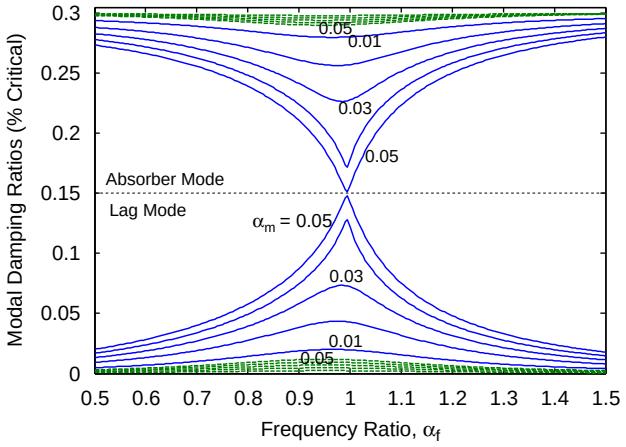

Fig. 5. Modal damping ratios vs frequency ratio, α_f ($\bar{a} = 0.3$ and $\zeta_a = 0.3$): — radial absorber, ------ chordwise absorber.

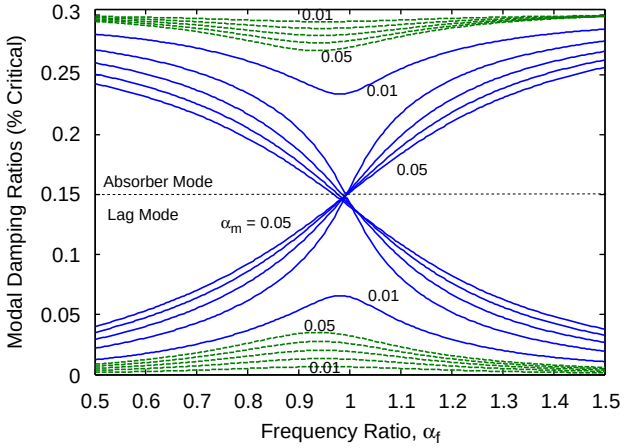

Fig. 6. Modal damping ratios vs frequency ratio, α_f ($\bar{a} = 0.5$ and $\zeta_a = 0.3$): — radial absorber, ------ chordwise absorber.

observed that the maximum damping transferred to the lag mode is 15% (one half the damping in the absorber mode) when $\alpha_f = 1$. For an inboard location of the absorber (Fig. 5), the actual damping in the lag mode depends on the absorber mass ratio, α_m, and while the ceiling value of 15% is reached for $\alpha_m = 5\%$, the damping in the lag mode is lower for smaller values of absorber mass ratio. As the absorber moves to mid-span and outboard locations (Figs. 6 and 7), the damping levels in the lag mode reach the ceiling value of 15% even for smaller absorber mass ratios. In fact, for $\bar{a} = 0.7$ (Fig. 7), even with an absorber mass that is only 1% of the blade mass, a maximum of 15% damping in the rotor lag mode can be achieved. The lag mode damping with the chordwise absorber is considerably lower, in all cases. For the inboard location ($\bar{a} = 0.3$, Fig. 5) a maximum of 1.1% damping is observed in the lag mode, for the mid-span location ($\bar{a} = 0.5$, Fig. 6) a maximum of 3.3% damping is observed, and for the outboard location ($\bar{a} = 0.7$, Fig. 7) a maximum of 7.5% damping is observed—but only for the highest absorber mass ratio ($\alpha_m = 5\%$) considered. For lower values of α_m the lag damping with the chordwise

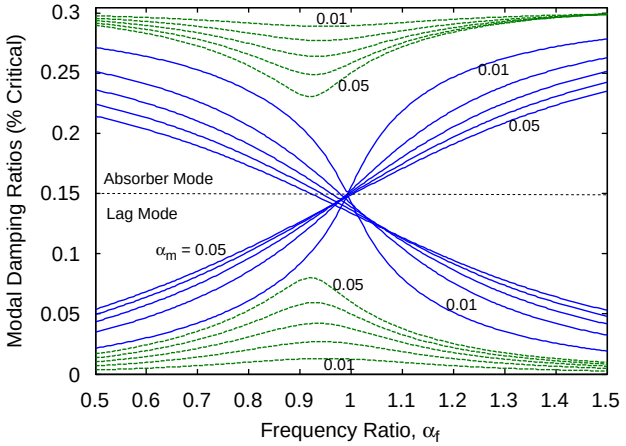

Fig. 7. Modal damping ratios vs frequency ratio, α_f ($\bar{a} = 0.7$ and $\zeta_a = 0.3$): — radial absorber, ------ chordwise absorber.

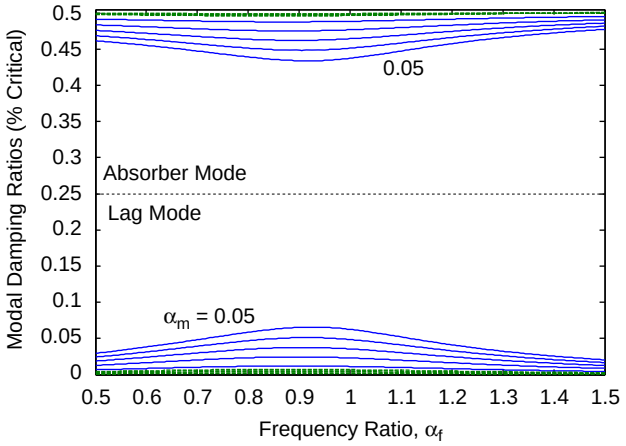

Fig. 8. Modal damping ratios vs frequency ratio, α_f ($\bar{a} = 0.3$ and $\zeta_a = 0.5$): — radial absorber, ------ chordwise absorber.

absorber considerably decreases. In contrast, with the radial absorber, damping of up to 15% is achieved with absorber mass ratios as low as 1%, and even when the absorber is not at the outermost spanwise location.

Figs. 8–13 show similar results for higher damped absorbers. Figs. 8–10 correspond to $\zeta_a = 0.5$, and Figs. 11–13 correspond to $\zeta_a = 0.7$. For the radial absorber, the maximum damping in the lag mode increases to 25% (when $\zeta_a = 0.5$) and to 35% (when $\zeta_a = 0.7$). However, to reach these higher ceiling values, larger absorber mass ratios and mid-span or outboard absorber locations are generally required. For example, it is seen in Figs. 8–10 that for the inboard location (Fig. 8) the ceiling damping in the lag mode could not be achieved for absorber mass ratios of up to 5% that were considered, but as the absorber moved to mid-span or outboard locations (Figs. 9 and 10) lag mode damping of up to 25% was observed for the higher mass ratios. In contrast, for the moderately damped absorber ($\zeta_a = 0.3$), the ceiling damping of 15% in the lag mode could be achieved even for an inboard absorber location (Fig. 5) and for low absorber mass ratios (Figs. 6 and 7). The performance of highly damped chordwise absorbers (in terms of their ability to transfer damping to the rotor lag mode) is very poor compared to that of the radial absorbers (as seen from Figs. 8–13). Overall, for chordwise absorbers, using the highest mass ratio allowed in this study ($\alpha_m = 5\%$) and the best spanwise location (outboard), a lightly damped absorber is the best choice (compare Figs. 7, 10 and 13). In contrast, for the radial absorber, if the absorber mass ratio is high and the absorber is situated outboard, an absorber with higher damping is able to transfer very high levels of damping to the rotor lag mode. This is clear when comparing Figs. 7, 10 and 13. With $\alpha_m = 5\%$, the highly damped absorber transfers up to 35% damping to the lag mode (Fig. 13), while the moderately and lightly damped absorbers transfer no more than 25% and 15% damping to the lag mode, respectively (Figs. 10 and 7).

By introducing a harmonic excitation force on the right hand side of the lag equation of motion for the coupled rotor lag—radial absorber system (Eq. (1)) and the rotor lag—chordwise absorber system (Eq. (2)), frequency response functions for the absorber dof, $\bar{\boldsymbol{x}}_{\boldsymbol{r}}$ and $\bar{x}_c$, and blade lag displacement, ζ, can be obtained. Of particular interest is the dynamic displacement amplitude of the absorber at a frequency of 1/rev, the dominant excitation frequency in forward flight.

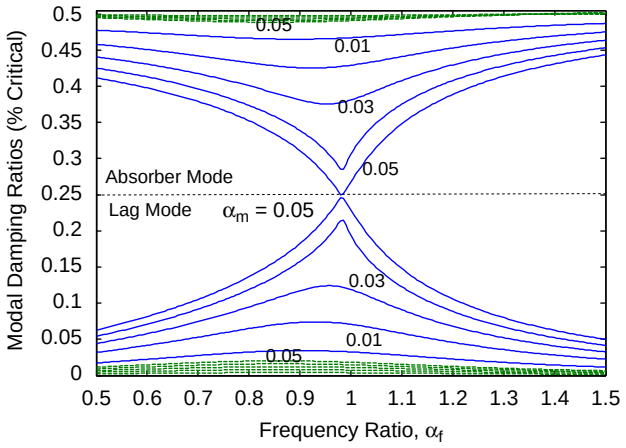

Fig. 9. Modal damping ratios vs frequency ratio, α_f ($\bar{a} = 0.5$ and $\zeta_a = 0.5$): — radial absorber, ------ chordwise absorber.

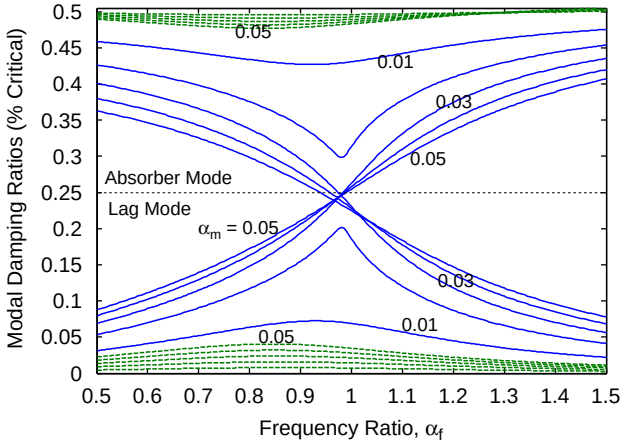

Fig. 10. Modal damping ratios vs frequency ratio, α_f ($\bar{a} = 0.7$ and $\zeta_a = 0.5$): — radial absorber, ------ chordwise absorber.

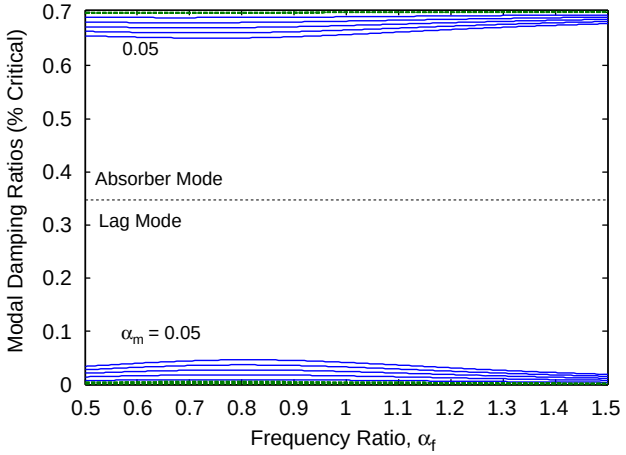

Fig. 11. Modal damping ratios vs frequency ratio, α_f ($\bar{a} = 0.3$ and $\zeta_a = 0.7$): — radial absorber, ------ chordwise absorber.

The radial absorber response is presented as a percentage of the blade radius, and the chordwise absorber response is presented as a percentage of the blade chord, both per degree of blade lead-lag motion amplitude. It is assumed that the blade has a notional chord length of 8% of the radius. The radial and chordwise absorber response results are shown in Figs. 15–23.

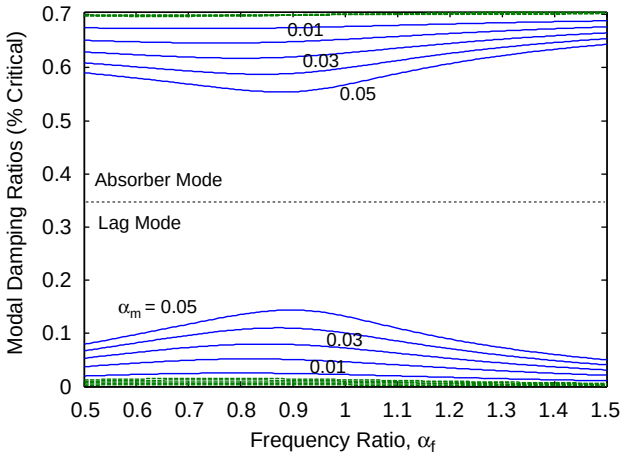

Fig. 12. Modal damping ratios vs frequency ratio, α_f ($\bar{a} = 0.5$ and $\zeta_a = 0.7$): — radial absorber, ------ chordwise absorber.

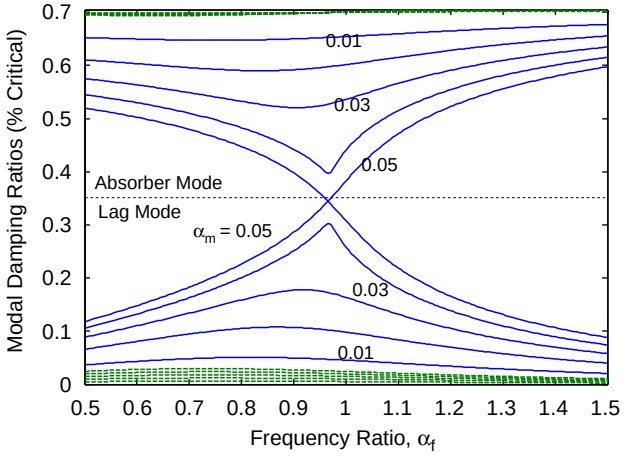

Fig. 13. Modal damping ratios vs frequency ratio, α_f ($\bar{a} = 0.7$ and $\zeta_a = 0.7$): — radial absorber, ------ chordwise absorber.

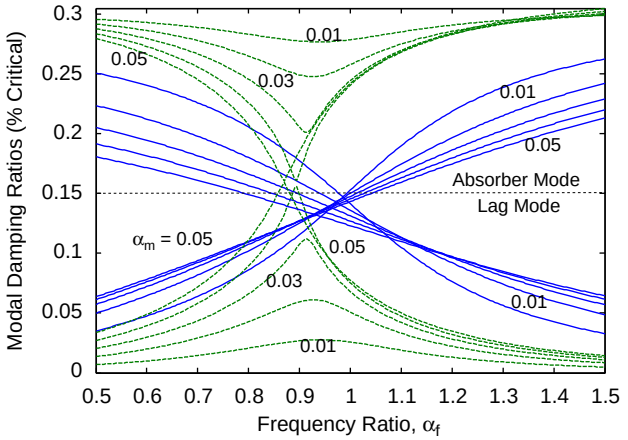

Fig. 14. Modal damping ratios vs frequency ratio, α_f ($\bar{a} = 1.0$ and $\zeta_a = 0.3$): — radial absorber, ------ chordwise absorber.

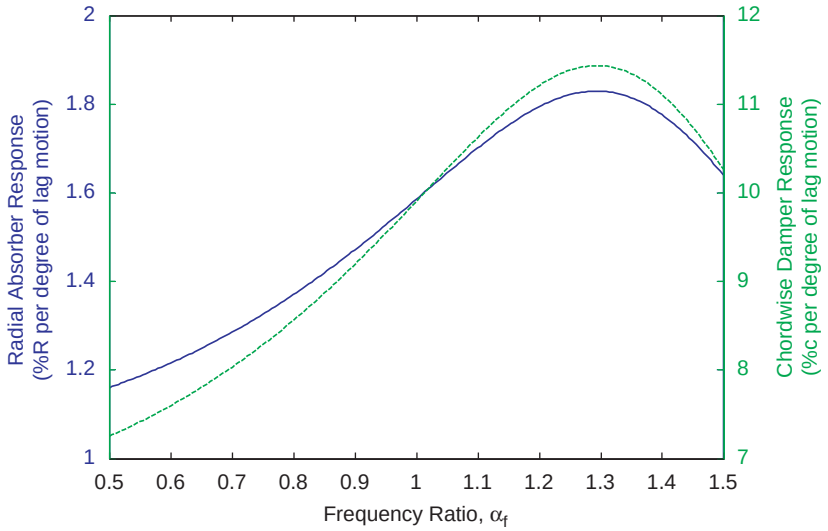

Fig. 15. 1/rev absorber amplitude per degree of lag motion ($\bar{a} = 0.3$ and $\zeta_a = 0.3$): — radial absorber, ------ chordwise absorber.

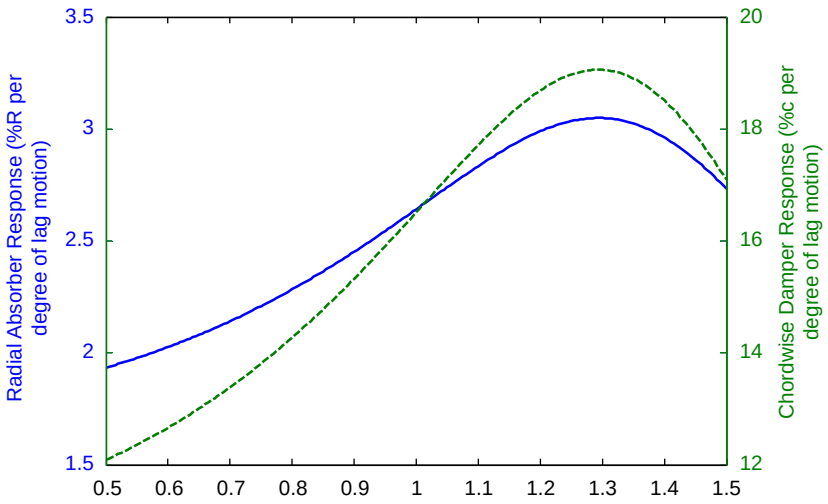

Fig. 16. 1/rev absorber amplitude per degree of lag motion ($\bar{a} = 0.5$ and $\zeta_a = 0.3$): — radial absorber, ------ chordwise absorber.

In general, it is observed that as the absorber moves outboard (compare Figs. 15–17, or 18–20, or 21–23), the absorber response amplitude increases. However, outboard absorbers were seen to introduce more lag damping than inboard absorbers. For a moderately damped absorber ($\zeta_a = 0.3$) at an outboard spanwise location ($\bar{a} = 0.7$), the periodic response amplitude of the radial absorber was about 4% blade radius and that of the chordwise absorber was about 25% chord, per degree of blade lead-lag motion amplitude (as seen in Fig. 17). If the chord length is a smaller fraction of the radius, the response amplitude of the chordwise absorber becomes an even greater percentage of the chord length. As the absorber damping increases, the periodic absorber response amplitude generally decreases (compare Figs. 18–20 for $\zeta_a = 0.5$, and Figs. 21–23 for $\zeta_a = 0.7$, to Figs. 15–17 for $\zeta_a = 0.3$). While highly damped chordwise absorbers were not particularly effective in augmenting lag damping, highly damped radial absorbers at outboard locations performed well. Thus a highly damped, outboard radial absorber may be an interesting possible candidate design to introduce high lag damping while having limited periodic response.

Recently, rotor lag damping augmentation using a chordwise absorber located at the tip of the rotor blade has been considered [21–24]. Fig. 14 shows simulation results for the chordwise and radial absorbers located at the rotor tip, for the case of absorber damping ratio, $\zeta_a = 0.3$. As seen in Fig. 14, at this location, the chordwise absorber is able to achieve approximately 15% lag mode damping when the absorber mass is 4–5% of the blade mass. With the radial absorber smaller mass ratios, as low as 1% of the blade mass, result in similar damping levels in the rotor lag mode. It should be noted that a radial absorber "at" the blade tip is impractical (stroke requirements would necessitate that the "absorber device" extend beyond the blade tip and it would no longer be "embedded" in the blade). However, the radial absorber even at mid-span

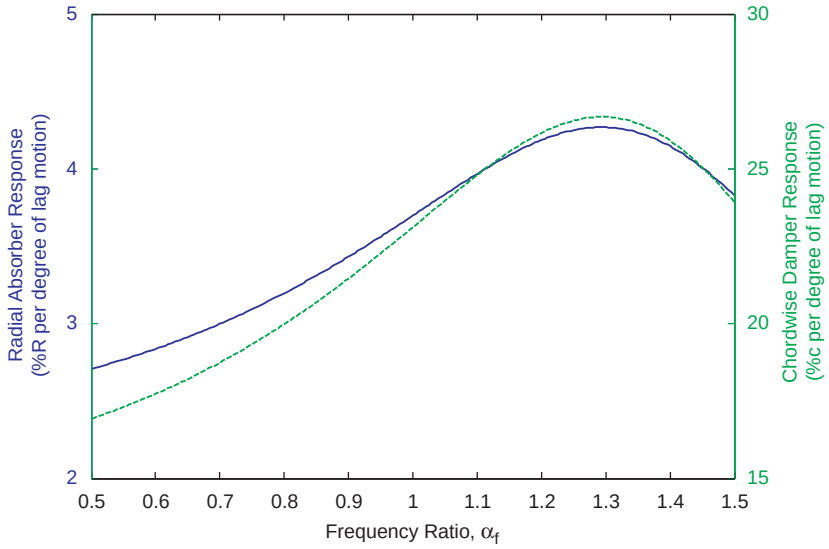

Fig. 17. 1/rev absorber amplitude per degree of lag motion ($\bar{a} = 0.7$ and $\zeta_a = 0.3$): — radial absorber, ------ chordwise absorber.

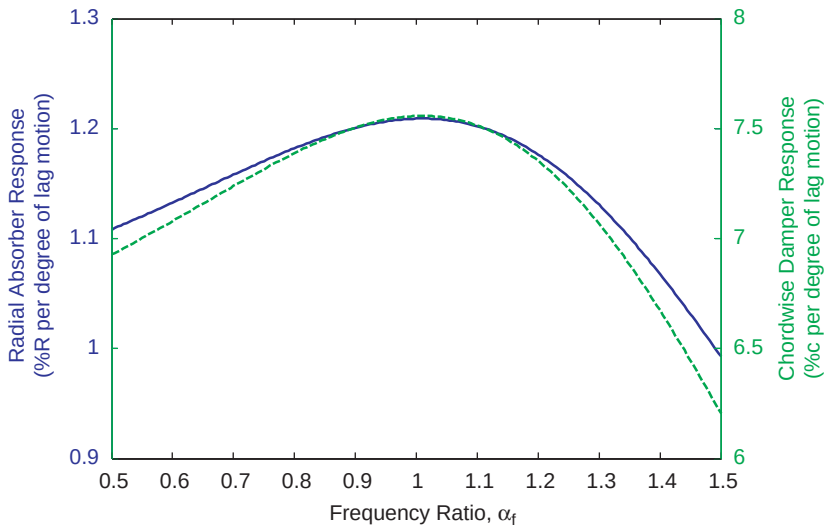

Fig. 18. 1/rev absorber amplitude per degree of lag motion ($\bar{a} = 0.3$ and $\zeta_a = 0.5$): — radial absorber, ------ chordwise absorber.

($\bar{a} = 0.5$) and at 70% span ($\bar{a} = 0.7$) transferred as much damping to the lag mode with smaller absorber mass ratios of $\alpha_m = 1$–2% (Figs. 6 and 7) as a chordwise absorber at the tip might. Fig. 24 shows that for the chordwise absorber at the tip, its chordwise motion amplitude (periodic response) per degree of blade lag motion is over $\pm 37\%$ of the chord, which may again not be feasible in an "embedded" configuration. For modern rotors with advanced tips incorporating taper and reduced thickness, an embedded chordwise absorber at the blade tip becomes even more impractical.

5. Radial absorber mass static displacement under centrifugal load

The results shown in Figs. 15–24 consider only the dynamic component of the absorber response. However, the total response of the absorber contains a static component and a dynamic component. A major factor in the implementation of a radial absorber concept is the large centrifugal force field in which the absorber will be required to operate. The static displacement of the radial vibration absorber due to the centrifugal force is dependent on the rotor speed, the radial offset of the absorber from the hub, the absorber mass, and the absorber spring stiffness as

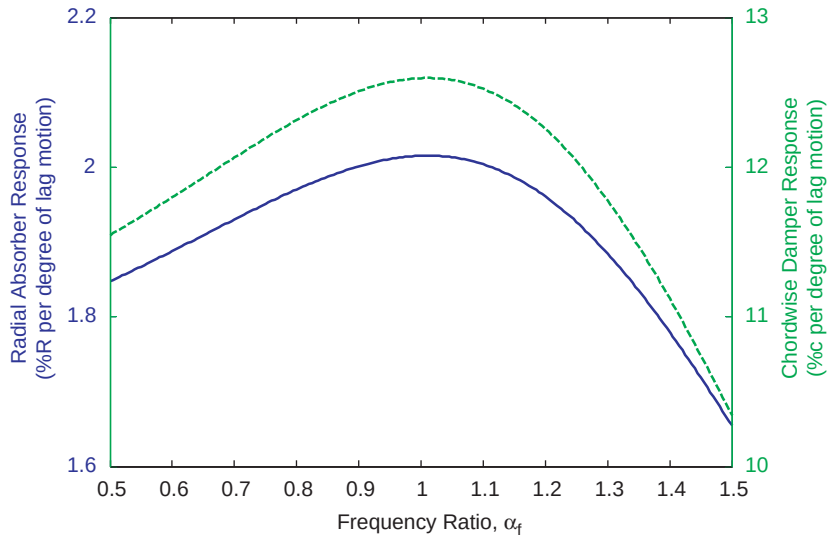

Fig. 19. 1/rev absorber amplitude per degree of lag motion ($\bar{a} = 0.5$ and $\zeta_a = 0.5$): — radial absorber, ------ chordwise absorber.

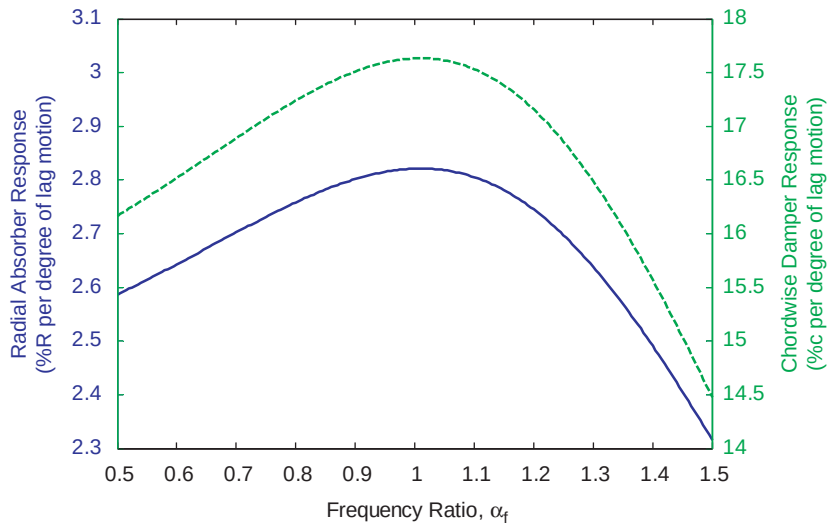

Fig. 20. 1/rev absorber amplitude per degree of lag motion ($\bar{a} = 0.7$ and $\zeta_a = 0.5$): — radial absorber, ------ chordwise absorber.

shown in Eq. (5) below

$$\bar{x}_{r_{static}} = \frac{\bar{a}\Omega^2}{\frac{k_a}{m_a} - \Omega^2} = \frac{\bar{a}\Omega^2}{\omega_a^2} = \frac{\bar{a}}{\alpha_f^2 \nu_\zeta^2}. \tag{5}$$

Using the spring stiffness required to achieve the desired tuning to the lag natural frequency ($\alpha_f = 1$) results in the prediction of an unrealistically large static displacement. In practice, either the absorber spring would fail, or the absorber mass would essentially become "pegged" against an outer constraint in the rotor blade. This problem could potentially be overcome in one of two ways. First, an absorber spring with a frequency-dependent stiffness could be used (with a high static stiffness to withstand the centrifugal force, but a low dynamic stiffness to achieve the desired tuning to the lag frequency of the blade). Alternatively, a nonlinear softening spring could be used such that the large initial stiffness results in modest deflection under centrifugal loading but the softening of the spring thereafter allows for dynamic motion and energy dissipation (the tangent stiffness of the softer part is selected such that the absorber is dynamically tuned to the rotor lag frequency).

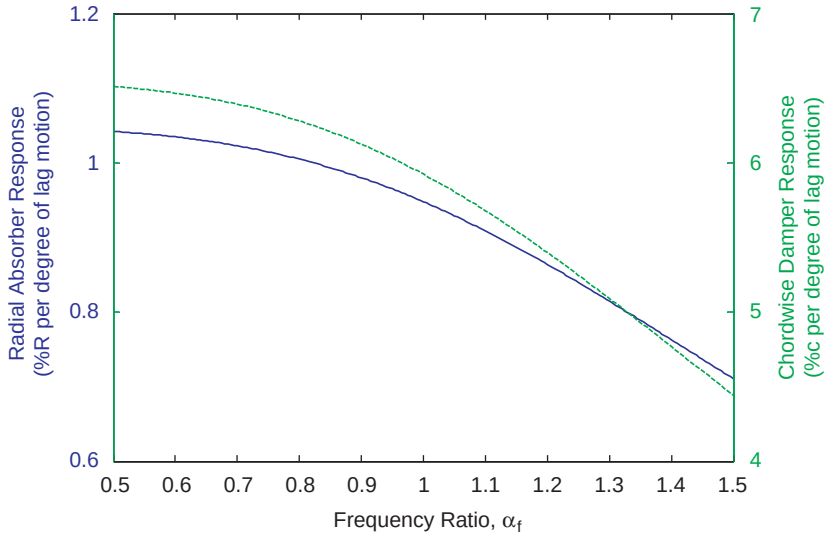

Fig. 21. 1/rev absorber amplitude per degree of lag motion ($\bar{a} = 0.3$ and $\zeta_a = 0.7$): — radial absorber, ------ chordwise absorber.

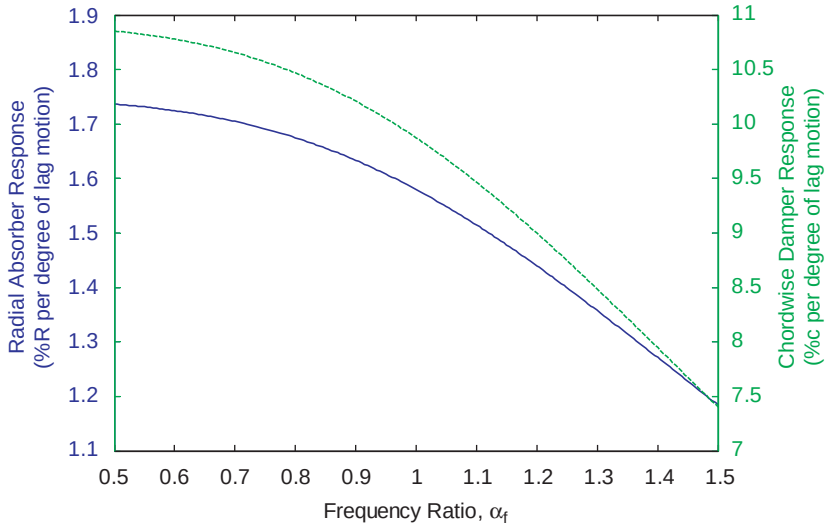

Fig. 22. 1/rev absorber amplitude per degree of lag motion ($\bar{a} = 0.5$ and $\zeta_a = 0.7$): — radial absorber, ------ chordwise absorber.

The force vs displacement of a proposed piecewise nonlinear spring is shown in Fig. 25. This type of spring would have a large stiffness over a given displacement of the spring to withstand the large centrifugal force. The stiffness would decrease for the absorber to be dynamically tuned at larger spring displacements to allow absorber dynamic motion and energy dissipation. The piecewise stiffness of the absorber could be constructed in the following manner. First, a desired static displacement of the absorber is selected, and the static stiffness of the absorber spring is determined using

$$k_{a_{static}} = m_a\left(1 + \frac{\bar{a}}{\bar{x}_{r_{static}}}\right)\Omega^2. \tag{6}$$

At the chosen static displacement, the stiffness of the absorber spring changes from the stiffness calculated in Eq. (6) to the stiffness determined from the tuning requirements of the system. This stiffness is determined such that the natural frequency of the absorber is equal to the lag natural frequency at the desired RPM, using Eq. (7)

$$k_a = m_a(1 + \upsilon_\zeta^2)\Omega^2. \tag{7}$$

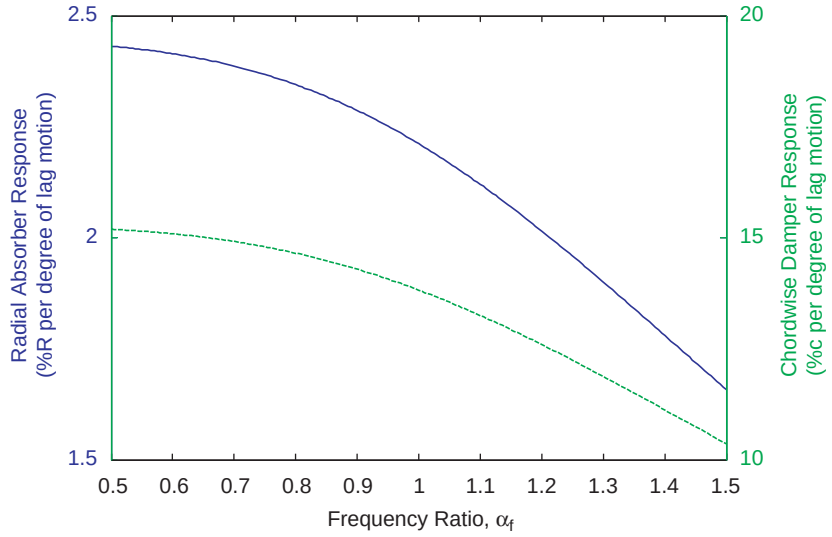

Fig. 23. 1/rev absorber amplitude per degree of lag motion ($\bar{a} = 0.7$ and $\zeta_a = 0.7$): — radial absorber, ------ chordwise absorber.

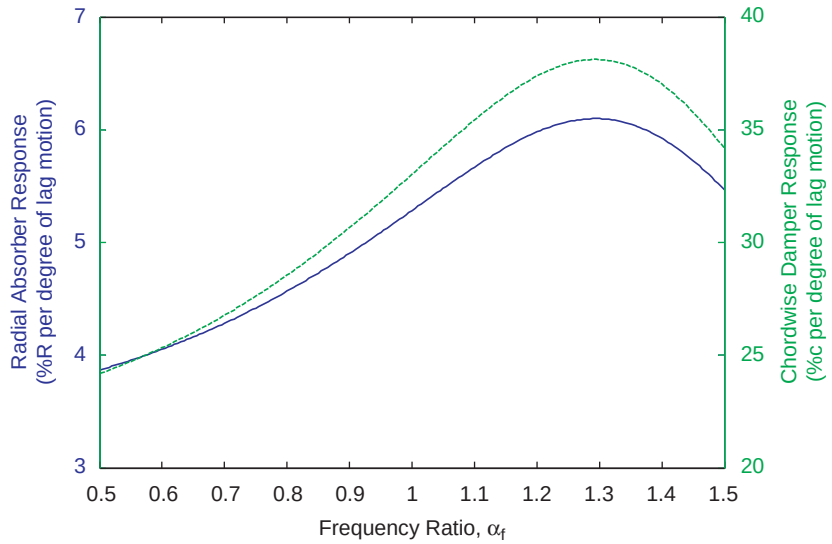

Fig. 24. 1/rev absorber amplitude per degree of lag motion ($\bar{a} = 1.0$ and $\zeta_a = 0.3$): — radial absorber, ------ chordwise absorber.

6. Buckling beam as a nonlinear spring for the radial absorber

A column under a compressive loading can be used as a nonlinear spring displaying a very high initial stiffness, which reduces significantly at higher loading levels approaching the critical buckling load. Such a column, designed to operate in compression and in the post-buckled state is referred to as an Euler spring. This type of nonlinear spring has been considered for use in vertical vibration isolation systems [28–32] which need a soft spring for low resonant frequency and good isolation characteristics, but must be able to support the mass in the presence of gravity without excessive static deformation. A linear spring that is soft enough for good isolation characteristics would result in large deformation under gravitational force. Fig. 26 shows the typical force vs displacement characteristics of an Euler spring. The critical buckling load, as well as the nonlinear force vs displacement profile, depends on the column length, flexural bending stiffness, boundary conditions and the initial curvature of the column.

Fig. 27 shows a schematic sketch of a radial absorber with the absorber mass attached to the tip of the Euler spring, configured along the span of the blade within the leading edge spar. The system could be designed so that the large initial stiffness results in only a small radial displacement of the absorber mass under the centrifugal force, but the reduced stiffness of the compressed column allows for the absorber to be tuned to the rotor lag natural frequency for effective transfer of damping to the lag mode.

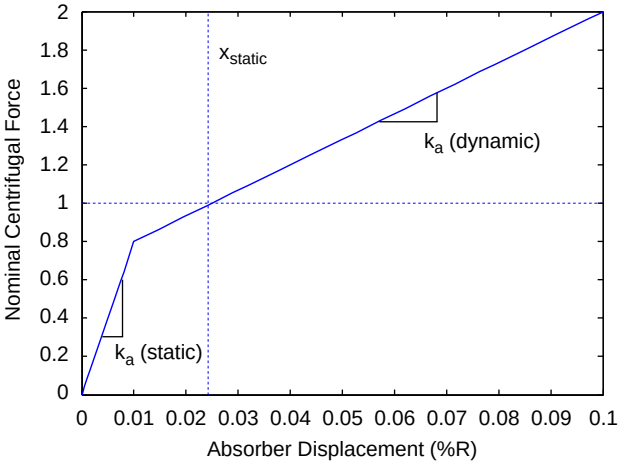

Fig. 25. Nonlinear piecewise spring stiffness.

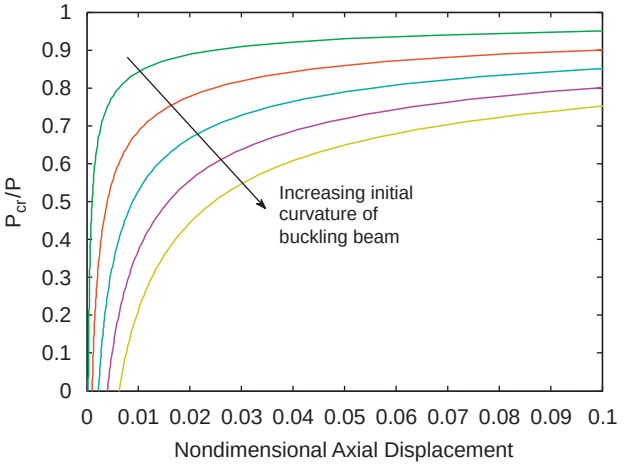

Fig. 26. Force vs displacement for a buckling beam.

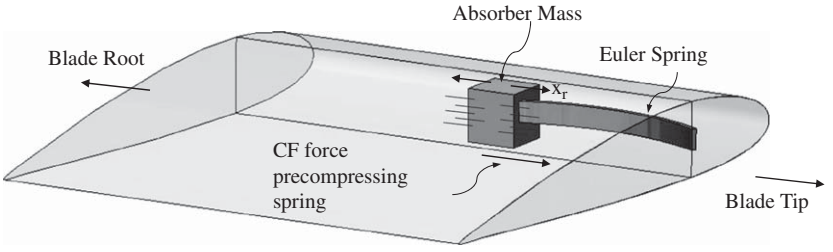

Fig. 27. Radial absorber with Euler spring.

7. Chordwise absorber and centrifugal load

For the chordwise absorber, the static displacement can be determined using the equation given below

$$\bar{x}_{c_{static}} = \frac{\bar{a}_c \Omega^2}{\frac{k_a}{m_a} - \Omega^2} = \frac{\bar{a}_c \Omega^2}{\omega_a^2} = \frac{\bar{a}_c}{\alpha_f^2 \nu_\zeta^2}. \tag{8}$$

Eq. (8) gives the static displacement of the chordwise absorber nondimensionalized by the blade chord if the offset, $\bar{a}_c$, of the absorber relative to the feathering axis is also nondimensionalized by the blade chord.

In Ref. [22] it was emphasized that for chordwise offsets, $\bar{a}_c$ in excess of 10% of the blade chord, the static displacement under the chordwise component of the centrifugal load could be unacceptably large. For this reason, development of a Fluidlastic® chordwise vibration absorber was pursued [23,24] which could provide a high static stiffness and a lower dynamic stiffness.

8. Conclusions

In this paper the potential of radial and chordwise damped vibration absorbers embedded in the rotor blade have been compared for rotor lag damping augmentation. The comparisons have been made on the same rotor and over a similar range of absorber parameters. Further, the 1/rev periodic response amplitude of the absorber mass per degree of blade lead-lag motion has been compared for both absorber concepts. Results show that the radial absorber, which transfers damping to the rotor blade lag mode via Coriolis coupling, is more effective in transferring damping to the rotor blade lag mode. It was shown that for the absorber parameters considered for the radial absorber, the chordwise damper cannot achieve the same levels of damping transferred to the lag mode as the radial absorber. To achieve these levels of lag damping, the chordwise damper must either use a much larger mass or be positioned further outboard on the rotor blade. Additionally, the chordwise damper has a significant restriction on stroke length. The radial absorber is also potentially less susceptible to aeroelastic instabilities and dynamic pitch-link loads as it does not involve the chordwise motion of the blade center of gravity. However, one disadvantage of the radial absorber as compared with the chordwise damper is the static displacement of the radial absorber due to the extremely large centrifugal force. This will be a major consideration in the design of the radial vibration absorber.

Appendix A. Derivation of the 2-dof equations of motion for the radial absorber

The differential equations of motion for the blade and radial absorber system are derived using Newtonian mechanics. The forces and moments acting on the blade are listed in Table A.1 and depicted in Fig. A.1. The radial forces acting on the absorber are listed in Table A.2 and depicted in Fig. A.2. The nonlinear terms deriving from Table A.1 were analyzed and found to be of much smaller magnitude than the linear terms and were neglected.

To obtain the blade equation of motion, moments are summed about the lag hinge, resulting in the following equation:

$$\left(\int_e^R m(r-e)^2\,\mathrm{d}r + m_a a^2\right)\ddot{\zeta} - 2m_a a\Omega\dot{x}_r + c_\zeta\dot{\zeta} + k_\zeta\zeta + \int_e^R mr\Omega^2(r-e)\zeta\frac{e}{r}\,\mathrm{d}r = \int_0^R F_\zeta r\,\mathrm{d}r. \tag{A.1}$$

Table A.1
Forces and moments acting on the blade.

Force/moment	Magnitude	Moment arm about lag hinge
Inertial force	$(mdr)(r-e)\ddot{\zeta}$	$(r-e)$
	$m_a(a+x_r)\ddot{\zeta}$	$(a+x_r)$
Coriolis force	$2m_a\Omega\dot{x}_r$	$(a+x_r)$
Centrifugal force	$(mr\Omega^2 dr)$	$(r-e)\zeta\frac{e}{r}$
Aerodynamic force	F_ζ	$(r-e)$
Spring moment	$k_\zeta\zeta$	–
Damping moment	$c_\zeta\dot{\zeta}$	–

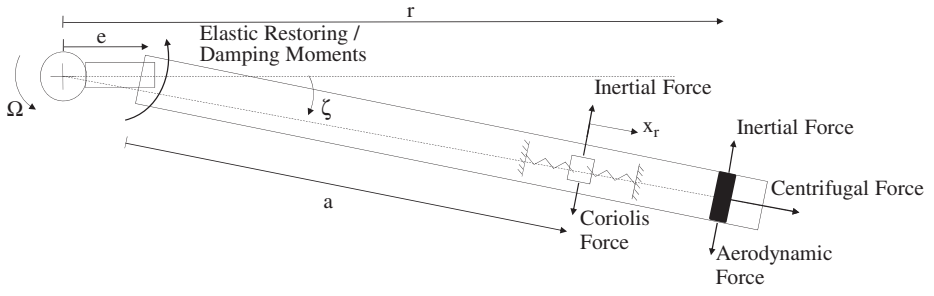

Fig. A.1. Forces and moments acting on the blade contributing to moments about the lag hinge.

Table A.2
Forces acting on absorber.

Force	Magnitude
Inertial force	$m_a\ddot{x}_r$
Coriolis force	$2m_a a\Omega\dot{\zeta}$
Centrifugal force	$m_a(a+x_r)\Omega^2$
Spring force	$k_a x_r$
Damping force	$c_a\dot{x}_r$

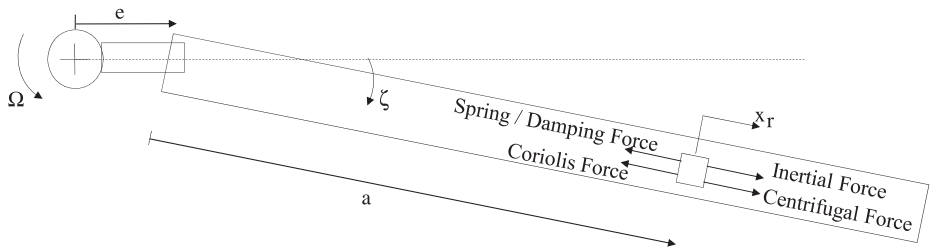

Fig. A.2. Forces acting on the absorber.

Dividing throughout by $\frac{1}{3}M(R-e)^2\Omega^2$(for a uniform blade), yields the nondimensional form of the lag equation

$$(1+3\alpha_m\bar{a}^2)\overset{**}{\zeta}-6\alpha_m\bar{a}\overset{*}{\bar{x}}_r+2\zeta_L v_\zeta\overset{*}{\zeta}+v_\zeta^2\zeta=\bar{M}_\zeta. \tag{A.2}$$

The absorber equation of motion is obtained by summing forces on the absorber in the radial direction:

$$m_a\ddot{x}_r+2m_a a\Omega\dot{\zeta}+c_a\dot{x}_r+(k_a-m_a\Omega^2)x_r=m_a a\Omega^2. \tag{A.3}$$

Like the lag equation, the absorber equation of motion can be nondimensionalized by dividing throughout by $m_a\Omega^2(R-e)$, resulting in the following equation:

$$\overset{**}{\bar{x}}+2\bar{a}\overset{*}{\zeta}+2\zeta_a\alpha_f\upsilon_\zeta\overset{*}{\bar{x}}+\alpha_f^2 v_\zeta^2\bar{x}=\bar{a}. \tag{A.4}$$

In Eqs. (A.2) and (A.4), the nondimensional rotating lag frequency is calculated by $v_\zeta^2=(k_\zeta/I_\zeta\Omega^2)+(eS_\zeta/I_\zeta)$. The blade and absorber equations of motion are coupled by the Coriolis terms, $2\bar{a}\overset{*}{\zeta}$ and $6\alpha_m\bar{a}\overset{*}{\bar{x}}_r$ (nondimensionalized). In matrix form, the nondimensional, coupled equations of motion can be written as shown in Eq. (A.5) below

$$\begin{bmatrix}1+3m_a\bar{a}^2 & 0\\ 0 & 1\end{bmatrix}\begin{Bmatrix}\overset{**}{\zeta}\\ \overset{**}{\bar{x}}_r\end{Bmatrix}+\begin{bmatrix}2\zeta_L v_\zeta & -6\alpha_m\bar{a}\\ 2\bar{a} & 2\zeta_a\alpha_f v_\zeta\end{bmatrix}\begin{Bmatrix}\overset{*}{\zeta}\\ \overset{*}{\bar{x}}_r\end{Bmatrix}+\begin{bmatrix}v_\zeta^2 & 0\\ 0 & \alpha_f^2 v_\zeta^2\end{bmatrix}\begin{Bmatrix}\zeta\\ \bar{x}_r\end{Bmatrix}=\begin{Bmatrix}\bar{M}_\zeta\\ \bar{a}\end{Bmatrix}. \tag{A.5}$$

References

[1] R.T. Lytwyn, W. Miao, W. Woitsch, Airborne and ground resonance of hingeless rotors, *Journal of the American Helicopter Society* 16 (2) (1971) 2–9.
[2] I. Chopra, Perspectives in aeromechanical stability of helicopter rotors, *Vertica* 14 (4) (1990) 457–508.
[3] R.A. Ormiston, Rotor-fuselage dynamics of helicopter air and ground resonance, *Journal of the American Helicopter Society* 36 (2) (1991) 3–20.
[4] F. Felker, B. Lau, S. McLaughlin, W. Johnson, Nonlinear behavior of an elastomeric lag damper undergoing dual frequency motion and its effect on rotor dynamics, *Journal of the American Helicopter Society* 32 (4) (1987).
[5] F. Gandhi, I. Chopra, An analytical model for a nonlinear elastomeric lag damper and its effect on aeromechanical stability in hover, *Journal of the American Helicopter Society* 39 (4) (1994) 59–69.
[6] F. Gandhi, I. Chopra, Analysis of bearingless main rotor aeroelasticity using an improved time-domain nonlinear elastomeric damper model, *Journal of the American Helicopter Society* 41 (3) (1996) 267–277.
[7] E. Smith, K. Govindswamy, M. Beale, Formulation, validation, and application of a finite element model for elastomeric lag dampers, *Journal of the American Helicopter Society* 41 (3) (1996) 247–255.
[8] C. Brackbill, et al., Application of a refined time domain elastomeric damper model to helicopter rotor aeroelastic response and stability, *Journal of the American Helicopter Society* 47 (3) (2002) 186–197.
[9] D. Kunz, Elastomer modeling for use in predicting helicopter lag damper behavior, *Journal of Sound and Vibration* 226 (3) (1999) 585–594.
[10] S. Marathe, F. Gandhi, K. Wang, Helicopter blade response and aeromechanical stability with a magnetorheological fluid based lag damper, *Journal of Intelligent Material Systems and Structures* 9 (4) (1998) 272–282.
[11] G. Kamath, N. Wereley, M. Jolly, Characterization of magnetorheological helicopter lag dampers, *Journal of the American Helicopter Society* 44 (3) (1999) 234–248.

[12] R. Snyder, G. Kamath, N. Wereley, Characterization and analysis of magnetorheological damper behavior under sinusoidal loading, *AIAA Journal* 39 (7) (2001).
[13] F. Gandhi, K.W. Wang, L. Xia, Magnetorheological fluid damper feedback linearization control for helicopter rotor application, *Smart Materials and Structures* 10 (2001) 96–103.
[14] Y. Zhao, Y. Choi, N. Wereley, Semi-active damping of ground resonance in helicopters using magnetorheological dampers, *Journal of the American Helicopter Society* 49 (4) (2004) 468–482.
[15] W. Hu, N.M. Wereley, L. Chemouni, P. Chen, Semi-active linear stroke magnetorheological fluid-elastic helicopter lag damper, *Journal of Guidance Control and Dynamics* 30 (2) (2007) 565–575.
[16] W.G. Bousman, An experimental investigation of the effects of aeroelastic couplings on aeromechanical stability of a hingeless rotor helicopter, *Journal of the American Helicopter Society* 26 (1) (1981) 46–54.
[17] R.A. Ormiston, Investigations of hingeless rotor stability, *Vertica* 7 (2) (1983) 143–181.
[18] M.D. Zotto, R.G. Loewy, Influence of pitch-lag coupling on damping requirements to stabilize ground/air resonance, *Journal of the American Helicopter Society* 37 (4) (1992) 68–71.
[19] F. Gandhi, E. Hathaway, Optimized aeroelastic couplings for alleviation of helicopter ground resonance, *Journal of Aircraft* 35 (4) (1998) 582–590.
[20] E. Hathaway, F. Gandhi, Concurrent optimization of aeroelastic couplings and rotor stiffness for the alleviation of helicopter aeromechanical instability, *Journal of Aircraft* 38 (1) (2001) 69–80.
[21] H. Kang, E. Smith, G. Lesieutre, Experimental and analytical study of blade lag damping augmentation using chordwise absorbers, *Journal of Aircraft* 43 (1) (2006).
[22] H. Kang, Blade Lag Damping Using Embedded Chordwise Absorbers, PhD Thesis, The Pennsylvania State University, August 2001.
[23] J. Petrie, G. Lesieutre, E. Smith, Helicopter blade lag damping using embedded fluid elastic inertial dampers, *Proceedings of the 45th AIAA/ASME/ASCE/AHS/ASC Structures, Structural Dynamics and Materials Conference*, Palm Springs, CA, April 2004.
[24] J. Petrie, G. Lesieutre, E. Smith, Design and model testing of helicopter rotor blade lag fluid elastic embedded chordwise inertial dampers, *Presented at the American Helicopter Society 61st Annual Forum*, Grapevine, TX, June 1–3, 2005.
[25] L. Byers, F. Gandhi, Helicopter rotor lag damping augmentation based on a radial absorber and coriolis coupling, *Presented at the American Helicopter Society 61st Annual Forum*, Grapevine, TX, June 1–3, 2005.
[26] L. Byers, F. Gandhi, Rotor blade with radial absorber (Coriolis Damper)—loads evaluation, *Presented at the American Helicopter Society 62nd Annual Forum*, Phoenix, AZ, May 9–11, 2006.
[27] L. Byers, Helicopter Rotor Lag Damping Augmentation Based on a Radial Absorber and Coriolis Coupling, PhD Thesis, The Pennsylvania State University, August 2006.
[28] J. Winterflood, T. Barber, D. Blair, Mathematical analysis of an Euler spring vibration isolator, *Physics Letters A* 300 (2002) 131–139.
[29] J. Winterflood, D. Blair, B. Slagmolen, High performance vibration isolation using springs in Euler column buckling mode, *Physics Letters A* 300 (2002) 122–130.
[30] E. Chin, et al., Low frequency vertical geometric anti-spring vibration isolators, *Physics Letters A* 336 (2005) 97–106.
[31] L. Virgin, R. Davis, Vibration isolation using buckled struts, *Journal of Sound and Vibration* 260 (5) (2003) 965–973.
[32] J. Ji, C. Hansen, Non-linear response of a post-buckled beam subjected to a harmonic axial excitation, *Journal of Sound and Vibration* 227 (2) (2000) 303–318.